




Article

Methods for Mathematical Analysis of Simulated and Real Fractal Processes with Application in Cardiology

Evgeniya Gospodinova ^{1,*}, Penio Lebamovski ¹, Galya Georgieva-Tsaneva ¹, Galina Bogdanova ²
and Diana Dimitrova ³¹ Institute of Robotics, Bulgarian Academy of Science, 1113 Sofia, Bulgaria² Institute of Mathematics and Informatics, Bulgarian Academy of Science, 1113 Sofia, Bulgaria³ Faculty of Public Health, Medical University "Prof. Dr. P. Stoyanov"-Varna, 9000 Varna, Bulgaria

* Correspondence: jenigospodinova@abv.bg

Abstract: In the article, a comparative analysis is performed regarding the accuracy parameter in determining the degree of self-similarity of fractal processes between the following methods: Variance-Time plot, Rescaled Range (R/S), Wavelet-based, Detrended Fluctuation Analysis (DFA) and Multifractal Detrended Fluctuation Analysis (MF DFA). To evaluate the methods, fractal processes based of Fractional Gaussian Noise were simulated and the dependence between the length of the simulated process and the degree of self-similarity was investigated by calculating the Hurst exponent ($H > 0.5$). It was found that the Wavelet-based, DFA and MF DFA methods, with a process length greater than 2^{14} points, have a relative error of the Hurst exponent is less than 1%. A methodology for the Wavelet-based method related to determining the size of the scale and the wavelet algorithm was proposed, and it was investigated in terms of the exact determination of the Hurst exponent of two algorithms: Haar and Daubechies with different number of coefficients and different values of the scale. Based on the analysis, it was determined that the Daubechies algorithm with 10 coefficients and scale ($i = 2, j = 10$) has a relative error of less than 0.5%. The three most accurate methods are applied to the study of real cardiac signals of two groups of people: healthy and unhealthy (arrhythmia) subjects. The results of the statistical analysis, using the t-test, show that the proposed methods can distinguish the two studied groups and can be used for diagnostic purposes.

Keywords: fractal process; Hurst exponent; multifractal process; RR time series**MSC:** 37M10

Citation: Gospodinova, E.; Lebamovski, P.; Georgieva-Tsaneva, G.; Bogdanova, G.; Dimitrova, D. Methods for Mathematical Analysis of Simulated and Real Fractal Processes with Application in Cardiology. *Mathematics* **2022**, *10*, 3427. <https://doi.org/10.3390/math10193427>

Academic Editor: Dumitru Baleanu

Received: 1 August 2022

Accepted: 16 September 2022

Published: 21 September 2022

Publisher's Note: MDPI stays neutral with regard to jurisdictional claims in published maps and institutional affiliations.



Copyright: © 2022 by the authors. Licensee MDPI, Basel, Switzerland. This article is an open access article distributed under the terms and conditions of the Creative Commons Attribution (CC BY) license (<https://creativecommons.org/licenses/by/4.0/>).

1. Introduction

A number of studies conducted in recent years have shown that many systems in nature generate time series with fractal behaviour [1–6]. Examples of such time series are: series of intervals between consecutive heartbeats [2,3,7], economic data on exchange rates [4], electricity prices [5], geophysical data on temperature, precipitation, tides [6,8–10], etc. For the analysis of this type of processes, methods are applied that allow the determination of the global characteristics of the processes as well as the peculiarities of their local structures. An important characteristic of these methods for analysing fractal processes is that they are fundamental and can be applied to time series from different areas: teletraffic engineering, medicine, geography, economy and more.

The concept of a fractal was first introduced by Benoit Mandelbrot in areas such as hydrology and geophysics. The word fractal is derived from the latin word fractus, which means consisting of fragments. At present, there is no strict and generally accepted definition of fractal, although Mandelbrot uses several conditional definitions. One of them, introduced in [11], reads the following: "The fractal is a set for which the Hausdorff-Besicovitch dimension strictly exceeds the topological dimension." The essence of this definition is to separate the class of highly broken objects for which there is no accurate

topological dimension. For example, there are curves that have a topological dimension equal per unit, but they are curved in a very complicated way, such as: the curves of Peano, the trajectory of a Brown particle and others. This definition, although strictly, excludes many physical fractals and is therefore less used. Another definition of fractal is [11]: “A fractal is an irregular geometric shape that can be divided into parts in such a manner that the shape of each part resembles the shape of the whole.” This definition emphasizes that the distinctive feature of the fractal is self-similarity.

A fractal processes has the following basic properties:

- Self-similarity—the fractal order is self-similarity if it can decompose into smaller parts, each of which is similar to the main one. The degree of self-similarity can be determined by the Hurst exponent.
- Fractal dimension (D)—this is a non-integer value located between the Euclidean and the topological dimensions [12].

Determining the fractal dimension of signals, as well as the degree of self-similarity, by calculating the Hurst exponent, is important in the study of fluctuations in time series. With these two parameters, it is possible to obtain information about the long-term correlations of the signals and, accordingly, to predict their behavior. These two parameters are connected to the expression $D = 2 - H$ [13] from which it follows that it is sufficient to determine only one of them. The present paper focuses on the determination of the Hurst exponent. This parameter can take values in the interval (0,1). If the value of the Hurst parameter is $0 < H < 0.5$, then the process is called anti-persistent, which means that growth in the past means decline in the future and vice versa. For $H = 0.5$, the process is neither persistent nor anti-persistent and thus a current value of the time series does not affect any of its future values. Such processes are called Markov processes. If $0.5 < H < 1.0$, it means the presence of fractal properties in the process. These processes are called persistent, i.e., if the increases were positive for some time in the past, then it is expected that in the future there will also be an average increase, i.e., the tendency to increase in the past means a tendency to increase in the future and conversely. The higher value of the Hurst exponent means that the trend is stronger. Therefore, based on the value of the Hurst exponent, it is possible to predict and predict the future values of a given time series based on present and past values. The focus in this paper is on simulating and analysing processes with Hurst exponent values in the interval (0.5,1.0).

Fractal processes are of two types: monofractal (self-similar) or multi-fractal [14,15]. A monofractal process is homogeneous in the sense that it has the same scaling properties both locally and globally and is characterized by a single scaling indicator, such as: the fractal dimension or the Hurst exponent. Unlike monofractal processes, multifractal processes decompose into a large number of homogeneous fractal subsets whose properties can be characterized by a spectrum of local Hurst exponents or fractal dimensions.

1.1. Related Work

The estimation of fractal processes is not a trivial task due to their time-varying behaviour. For this reason, these processes cannot be comprehensively described by statistical measurements, such as: mean value, standard deviation, and others. For this purpose, it is necessary to use mathematical methods created for the analysis of dynamic time series such as: Variance-time plot, Rescaled Range (R/S) analysis, Wavelet-based method, Detrended Fluctuation Analysis (DFA), Multifractal Detrended Fluctuation Analysis (MFDFA) and others. The interest in these methods of analysis led to the need to evaluate and test them according to well-defined criteria before being used for wide application in various fields of science.

In [14], the authors presented a comparative analysis of three methods, Variance-time plot, R/S analysis, Wavelet-based and concluded that the first two methods are not very accurate. These methods can only be used to show whether the studied process has a fractal behaviour and if it does, the methods can be used to approximately to determine the value of the Hurst exponent. The authors of the publication determine the Wavelet-based method

as an accurate method. Although the R/S method is not the most accurate, nowadays it is actively applied in the analysis of fractal processes in various scientific fields due to its easy of use [16–22].

As a result of the work on heartbeat dynamics described in [15], multifractal analysis has become a widely used tool for applied research, in cases where non-stationary processes are limited by the application of the classical analysis methods [23–27].

Accurate reference signals are required to evaluate fractal time series analysis methods. Fractal time series can be simulated by applying the models based on fractional Brownian motion (FBM) and fractional Gaussian noise (FGN). In this article, the FGN model is chosen to simulate fractal processes. This model is fully described by two parameters only, namely by a variance and Hurst exponent [14,28–31].

In recent years, there has been an active introduction of mathematical methods for fractal and multifractal analysis in medical practice. Many scientists have studied the complex nature of changes in the parameters of electrocardiographic signals using not only linear but also nonlinear methods [32,33]. The linear methods perform analysis in the time and frequency domain, while some of the nonlinear methods use the fractal approach in the analysis of cardiological data. According to the European and North American Society of Cardiology, the study of the applicability of these methods for the analysis of cardiological data is one of the important priority areas, which opens new perspectives for their future use in the diagnosis and prediction of cardiovascular diseases [34].

The authors of [35] advise physicians to interpret the results obtained from fractal and traditional heart rate variability analysis methods with caution, as they are still under investigation and the resulting measurements are not fully described as biomarkers for clinical use.

1.2. Purpose and Objective of the Article

The purpose of this article is to perform a comparative analysis between the following methods: Variance-time plot, Rescaled Range analysis(R/S), Wavelet-based method, DFA and MFDEFA in terms of the accuracy parameter when determining the value of the Hurst exponent. The most accurate methods determined will be used to analyse real cardiac data. To achieve the set goal, the following tasks have been formulated:

1. Simulate an exact FGN-based self-similar (fractal) process by applying Hosking's algorithm.
2. Comparative analysis of the following 5 methods: Rescaled Range analysis (R/S), Variance-time plot, Wavelet-based method, DFA, MFDEFA to determine the value of the Hurst exponent with respect to the accuracy parameter.
3. Study of cardiac signals of two groups of patients by applying the most accurate methods of analysis.

2. Materials and Methods

To study fractal processes, methods are used that, based on one or more statistical properties, determine the degree of self-similarity (Hurst exponent). Due to the wide variety of statistical methods and due to the fact that so far there is no universally recognized methodology for determining the degree of self-similarity, an analysis and evaluation of the most frequently used methods in terms of their main parameters is necessary. The most accurate possible determination of the degree of self-similarity is of great importance in the study of simulated and real fractal processes.

2.1. Hosking's Algorithm for Simulation Modeling of Fractal Processes

The Hosking algorithm (also known as the Durbin-Levinson algorithm) generates an exact self-similar process based on the FGN [36–38]. The main idea of the algorithm is to generate a self-similar sequence by using a zero-mean Gaussian process. Each generated point has a mean and variance dependent on the previous generated values. It is necessary to know the autocorrelation function of the process when calculating the point values.

The coefficients of the autocorrelation function of an exactly self-similar process in the broad sense with parameter H ($0.5 < H < 1.0$) are determined by the following formula [10]:

$$r_k = \frac{\sigma^2}{2} \left[(k+1)^{2H} - 2k^{2H} + (k-1)^{2H} \right], \quad k = 0, 1, 2, \tag{1}$$

where:

- r_k are autocorrelation coefficients;
- σ is the variance;
- H is the Hurst exponent.

The algorithm for simulating an exact self-similar (fractal) process $\{X_1, X_2, \dots, X_n\}$ of length n points consists of the following steps:

Step 1: Calculation the coefficients of the autocorrelation function for n points using Formula (1).

Step 2: The X_1 value of the first element of the process is determined using the formula: $X_1 = \sqrt{r_0}Z_1$. The value of Z_1 is a random variable with a normal probability distribution $N(0,1)$.

Step 3: The following variables are defined:

$$\sigma_0^2 = r_0, \quad \phi_{11} = \frac{r_1}{r_0}, \quad \sigma_1^2 = \sigma_0^2 \left(1 - \phi_{11}^2 \right) \tag{2}$$

where:

- σ_0^2 and σ_1^2 are the variances of the first two elements of the generated process;
- ϕ_{11} is the correlation coefficient for the first element X_1 of the fractal process;
- r_0 and r_1 are the autocorrelation coefficients of the first two elements of the generated process.

Step 4: For $n = 2 \dots K$ the following coefficients and variables are calculated:

$$\phi_{n,n} = \left[r_n - \sum_{j=1}^{K-1} \phi_{n-1,j} r_{n-j} \right] / \sigma_{n-1}^2 \sigma_n^2 = \sigma_{n-1}^2 \left[1 - \phi_{n,n}^2 \right] \tag{3}$$

Step 5: For $j = 1, \dots, n-1$ the following calculations were performed:

$$\phi_{n,j} = \phi_{n-1,j} - \phi_{n,n} \phi_{n-1,n-j} \tag{4}$$

Step 6: To generate a fractal process $\{X_1, X_2, \dots, X_n\}$ the following formula is used:

$$X_{n+1} = \phi_{n,1}X_n + \dots + \phi_{n,n}X_1 + \sqrt{\sigma_n^2}Z_{n+1}, \quad n \geq 1 \tag{5}$$

where $\{Z_1, Z_2, \dots, Z_n\}$ are random variables with a normal probability distribution $N(0,1)$.

2.2. Methods for Determining the Hurst Exponent

2.2.1. Variance-Time Plot

Variance-Time plot [14] is based on the following property of fractal (self-similar) processes: the variance of the generalized stochastic process $X(m)$ decreases more slowly than the reciprocal of the size of the blocks (m) into which the process is divided:

$$\sigma^2(X^{(m)}) \sim cm^{2H-2} \tag{6}$$

where c is some finite positive constant.

The Variance-time plot consists in constructing the graphical relationship between Log(disperse) and Log(block size) and determining the slope of the regression line. The degree of self-similarity, i.e., the Hurst exponent, is determined by the following relationship:

$$\hat{H} = 1 - \frac{\hat{\beta}}{2} \tag{7}$$

where:

- $\hat{\beta}$ is the slope of the regression line;
- \hat{H} is the determined value of the Hurst exponent.

2.2.2. Rescaled Range Statistics

The algorithm of the Rescaled Range Statistics (R/S) method [14,39–41] for determining the degree of self-similarity calculates the range and standard deviation of the blocks into which the process is divided. For each block are calculated:

- The Range $R(n)$, which defines the differences between the min and max value of the sum of the deviation W_j from the mean value of the data for an area of n points, is given by the expression:

$$R(n) = \max(0, W_1, W_2, \dots, W_n) - \min(0, W_1, W_2, \dots, W_n) \tag{8}$$

where:

$$W_j = (X_1 + X_2 + \dots + X_j) - j\bar{X}(n), j = 1, 2, \dots, n \tag{9}$$

- Standard deviation $S(n)$:

$$S(n) = \sqrt{E(X_j - \mu)} \tag{10}$$

where μ is the mean of (X_1, X_2, \dots, X_j) [14].

Based on a regression model between the dependent variable Log(R/S) and the independent variable Log(block size), the following regression coefficients are determined by the method of least squares:

- $\hat{\beta}_0$ is the point where the regression line intersects the ordinate;
- $\hat{\beta}_1$ is the slope of the regression line.

The value of the Hurst exponent is determined by the following formula:

$$\hat{H} = \hat{\beta}_1 \tag{11}$$

2.2.3. Wavelet-Based Method

The wavelet-based method [14,42,43] uses the wavelet transform, which is suitable for studying fractal processes because the structure of wavelets is similar to the self-similar structure of fractal processes. The wavelet transform is known to be better than the Fourier transform for the following reasons:

- The Fourier transform is used to transform stationary processes from the frequency domain to the time domain, and the process is transformed as a sum of sinusoids with different frequencies. It cannot represent the information in the time domain.
- The wavelet transform can represent the process in the time and frequency domains simultaneously. It can transform both stationary and non-stationary processes without loss of information.

Wavelet transform algorithms are recursive and consist of two wavelet filters: low-pass and high-pass. After the low-pass filter, approximate information is obtained, and after the high-pass filter, detailed information is obtained. The approximating information obtained at the output of the low-pass filter becomes the input information for the next level of decomposition.

Wavelet algorithms consist of the following two components:

- A wavelet function ($\psi_{i,j}$) applied to the high-pass filter that is run two or more times and computes wavelet coefficients;
- A scalable function ($\phi_{i,j}$) relating the low-pass filter that creates a smoother version of the original data. The received data after the low-pass filter become input data for the next step of the algorithm.

The mathematical descriptions of the above functions are:

$$\phi_{i,j}(t) = 2^{-\frac{i}{2}} \phi_0(2^{-i}t - j), \quad i, j \in \mathbb{Z} \tag{12}$$

$$\psi_{i,j}(t) = 2^{-\frac{i}{2}} \psi_0(2^{-i}t - j), \quad i, j \in \mathbb{Z} \tag{13}$$

where:

- ϕ_0 is a scalable function;
- ψ_0 is the mother wavelet and originates from ϕ_0 .

Applying Multi-Resolution analysis to the input data x means representing x in each of the approximating subspaces V_i :

$$\text{approx}_i(t) = \sum_j a_x(i,j) \phi_{i,j}(t) \tag{14}$$

where the coefficient $a_x(i,j)$ is calculated by multiplying the input data x with $\phi_{i,j}$:

$$a_x(i,j) = \langle x, \phi_{i,j} \rangle \tag{15}$$

The approximating information approx_i is a rough approximation of the input data x to $\text{approx}_{(i-1)}$ and information is lost $\text{detail}_i(t) = \text{approx}_{i-1}(t) - \text{approx}_i(t)$. The detail information of the input data x is determined by a formula:

$$\text{detail}_i(t) = \sum_j d_x(i,j) \psi_{i,j}(t) \tag{16}$$

where the coefficient $d_x(i,j)$ is calculated by multiplying the input data x with $\psi_{i,j}$:

$$d_x(i,j) = \langle x, \psi_{i,j} \rangle \tag{17}$$

The input information x is represented as a sum of the approximating and detailed information:

$$x(t) = \text{approx}_N(t) + \sum_{i=1}^N \text{detail}_i(t) = \sum_j a_x(N,j) \phi_{N,j}(t) + \sum_{i=1}^N \sum_j d_x(i,j) \psi_{i,j}(t) \tag{18}$$

Equation (18) is called the wavelet decomposition of the signal x , and the coefficients $a_x(j,k)$ and $d_x(j,k)$ are determined by multiplying the input data with the scalable function $\phi_{i,k}$ and the wavelet function, respectively.

The wavelet-based method [14] for determining the Hurst exponent consists in determining the average value of the wavelet detail coefficients $|d_x(i,j)|^2$ for a given scale:

$$Y_x = \frac{1}{n_j} \sum_j |d_x(i,j)|^2 \tag{19}$$

where n_j is the number of wavelet coefficients for a given scale in the interval $[i,j]$, i.e. $n_j = 2^{-i} n$, and n is the number of the input points.

To determine the Hurst exponent, a discrete wavelet transform is performed relative to the studied process using a wavelet algorithm (Daubechies, Haar, etc.) [44–47] and the values of Y_x by Equation (19). A linear regression model is constructed, with the dependent variable being $\text{Log}(Y_x)$ and the independent variable being the scale in the interval $[i,j]$. The relationship between the two variables is linear if the process under study is fractal. The slope of the straight line is determined using the method of least squares. For fractal processes the slope β_1 is between 0 and 1, and the Hurst exponent is determined using the following relationship:

$$\hat{H} = \frac{1}{2}(1 + \hat{\beta}_1) \quad (20)$$

In order to determine the value of the Hurst exponent, it is necessary to perform a discrete wavelet transformation on the investigated process, proposing a wavelet algorithm and setting values for the (i,j) scale.

2.2.4. Detrended Fluctuation Analysis

The DFA method allows studying the structures of different types of non-stationary signals from the point of view of statistical self-similarity. The non-stationary dynamics of systems with time-varying characteristics limits the applicability of classical methods for spectral-correlation analysis. For this reason, for the study of long-term correlations in experimental data, the method of detrended fluctuation analysis (DFA) is most often used, which is described in detail in publications [7,32,33,48,49].

The DFA method has the following two characteristic features:

- Instead of using a decreasing correlation function, an increasing function is introduced, which provides a more reliable estimation of processes with long-term correlations, especially in the presence of noise and sample size limitations;
- An integral part of the calculation algorithm is the approximation and subsequent elimination of the low-frequency trend, which makes it possible to apply the method to both stationary and non-stationary processes without their prior filtering.

These circumstances determine the wide use of DFA, for example, in the processing of experimental data in physiology and medicine, as well as in various fields of physics. DFA is used for time series with a random structure, as well as to detect short-term correlations through the parameter α_1 and long-term correlations through α_2 . Initially, the entire process is divided into segments of equal size, and for each segment a regression line is formed by applying the method of least squares and the slope of the regression curve is determined. The parameter α_{all} is calculated for the whole process. This parameter is called the self-similar parameter and its value varies between 0.5 and 1.0 and is close to the value of the Hurst exponent.

The advantage of DFA over conventional methods such as spectral analysis lies in the fact that this type of analysis makes it possible to detect the self-similarity property of the process.

2.2.5. Multifractal Detrended Fluctuation Analysis

MF DFA is applied to analyse the complexity and non-uniformity based on the scaling behaviour of the studied time series. A detailed description of this method is presented in publications [50–52]. In this article, the relationship between the generalized Hurst exponent $H(q)$ and parameter q is used to study the fractal and multifractal properties of simulated and real fractal processes. The generalized Hurst exponent $H(q = 2) = H$ reflects the structural inhomogeneity of the signal. If $H(q)$ does not depend on q , the process is monofractal, otherwise it is multifractal. The parameter q can take any real value.

2.3. Data

Two types of data are used in the paper: simulated fractal processes and real cardiac signals.

The simulated fractal processes have been created using Matlab R2013b. The simulated processes have two input parameters: process length and Hurst exponent value. On the basis of the simulated fractal processes, a comparative analysis was performed between the five methods for determining the value of the Hurst exponent, and on the basis of the obtained results, the most optimal methods were determined in terms of the accuracy parameter. Real cardiac data (RR time series) were recorded with a Dynamic ECG Systems TLC9803 Holter device. Data from 48 patients diagnosed with arrhythmia and 48 healthy subjects were studied. The duration of the recordings are 24 h with approximately 100,000 RR time intervals.

3. Results and Discussion

3.1. Analysis of Simulated Data

In order to perform a comparative analysis between the methods used to determine the Hurst exponent, it is necessary to first determine the minimum length of the generated process in order to achieve more accurate results. Second, due to the fact that the wavelet-based method does not offer a methodology for determining the scale size and selection of the wavelet algorithm, in this paper, two wavelet algorithms are investigated and compared in terms of the accurate determination of the Hurst exponent: Haar and Daubechies.

3.1.1. Determining the Minimum Length of a Simulated Fractal Process

With the Hosking algorithm described above, fractal processes with varying degrees of self-similarity were generated. Figure 1 shows two generated processes with low and high degree of self-similarity: $H = 0.6$ and $H = 0.9$.

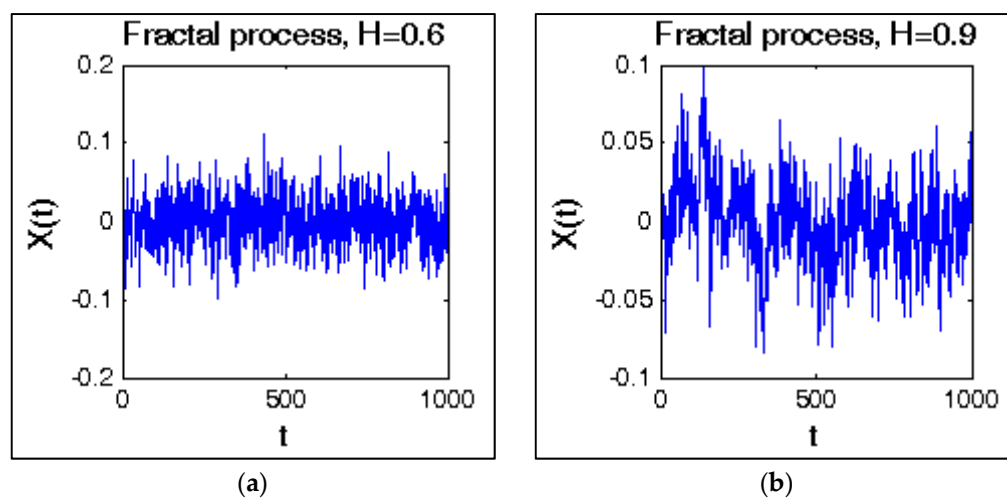


Figure 1. Simulated FGN fractal processes (a) $H = 0.6$ (b) $H = 0.9$.

When determining the minimum length of the fractal process, the dependence between the length of the simulated process and the Hurst exponent, determined through the five methods, was investigated. Due to the presence of a random component in the Hosking algorithm, 20 realizations of the process with different lengths were simulated: from 2^{12} (4096) to 2^{17} (131,072) points for the following 4 values of the Hurst input parameter: $H = 0.6, 0.7, 0.8$ and 0.9 . In the present work, it is assumed that the size of the generated fractal process is acceptable when the Relative Standard Error (RSE) of the Hurst exponent is less than 1%.

The results of the comparative analysis between the five methods are shown in Table 1. At different lengths of the process, the values of the Hurst exponent \hat{H} , and the RSE(%) were determined. Based on the obtained results, the following conclusions can be drawn:

1. Variance-time plot and R/S are not very accurate methods, as their RSE are in a wide range from 0.2% to 11.3%, and these methods can only be used to test whether the

- studied process is fractal or not, and if it is fractal, approximately to be determined the value of the Hurst exponent;
- The determined values of the Hurst exponent with the methods: Wavelet-based, DFA and MFDFA reach the input values of this parameter with a RSE of less than 1% for process lengths greater than 2^{14} (16,384) points. These three methods have a high degree of accuracy and can be used in the analysis of simulated and real processes;

Table 1. Comparative analysis between five statistical methods in determining the Hurst exponent at different FGN fractal process lengths.

Length (Points)	H = 0.6		H = 0.7		H = 0.8		H = 0.9	
	\hat{H} Mean \pm sd	RSE (%)	\hat{H} Mean \pm sd	RSE (%)	\hat{H} Mean \pm sd	RSE (%)	\hat{H} Mean \pm sd	RSE (%)
Variance-Time Plot								
2^{12}	0.611 \pm 0.07	2.56	0.703 \pm 0.04	1.27	0.783 \pm 0.08	2.28	0.848 \pm 0.21	5.54
2^{13}	0.541 \pm 0.09	3.72	0.639 \pm 0.17	5.95	0.736 \pm 0.21	6.38	0.834 \pm 0.33	8.85
2^{14}	0.534 \pm 0.13	5.44	0.626 \pm 0.21	7.50	0.713 \pm 0.32	10.03	0.798 \pm 0.41	11.49
2^{15}	0.604 \pm 0.06	2.22	0.691 \pm 0.10	3.24	0.771 \pm 0.11	3.19	0.835 \pm 0.28	7.07
2^{16}	0.578 \pm 0.08	3.09	0.664 \pm 0.19	6.40	0.744 \pm 0.22	6.61	0.835 \pm 0.35	9.37
2^{17}	0.582 \pm 0.07	2.69	0.671 \pm 0.18	6.00	0.761 \pm 0.15	4.41	0.840 \pm 0.27	7.19
Rescaled range (R/S) method								
2^{12}	0.645 \pm 0.21	7.28	0.730 \pm 0.12	3.68	0.809 \pm 0.04	1.11	0.873 \pm 0.11	2.82
2^{13}	0.609 \pm 0.08	2.94	0.694 \pm 0.03	0.97	0.775 \pm 0.11	3.20	0.841 \pm 0.19	5.05
2^{14}	0.607 \pm 0.05	1.84	0.690 \pm 0.05	1.62	0.768 \pm 0.13	3.78	0.851 \pm 0.20	5.26
2^{15}	0.620 \pm 0.09	3.25	0.681 \pm 0.08	2.63	0.780 \pm 0.10	2.87	0.851 \pm 0.21	5.52
2^{16}	0.596 \pm 0.04	1.50	0.687 \pm 0.06	1.95	0.763 \pm 0.16	4.69	0.853 \pm 0.19	4.98
2^{17}	0.601 \pm 0.02	0.74	0.703 \pm 0.01	0.32	0.771 \pm 0.14	4.06	0.856 \pm 0.17	4.44
Wavelet-based method (Daubechies algorithm with 10 coefficients)								
2^{12}	0.579 \pm 0.10	3.86	0.678 \pm 0.11	3.63	0.790 \pm 0.05	1.42	0.930 \pm 0.09	2.16
2^{13}	0.585 \pm 0.06	2.29	0.687 \pm 0.06	1.95	0.788 \pm 0.04	1.14	0.890 \pm 0.07	1.76
2^{14}	0.583 \pm 0.07	2.68	0.686 \pm 0.08	2.61	0.787 \pm 0.03	0.85	0.888 \pm 0.06	1.51
2^{15}	0.606 \pm 0.02	0.74	0.705 \pm 0.03	0.95	0.804 \pm 0.03	0.83	0.904 \pm 0.04	0.99
2^{16}	0.601 \pm 0.01	0.37	0.702 \pm 0.02	0.64	0.803 \pm 0.02	0.56	0.903 \pm 0.03	0.74
2^{17}	0.599 \pm 0.01	0.37	0.700 \pm 0.01	0.32	0.801 \pm 0.01	0.28	0.901 \pm 0.01	0.25
Detrended Fluctuation Analysis method								
2^{12}	0.615 \pm 0.09	3.27	0.715 \pm 0.10	3.13	0.814 \pm 0.12	3.39	0.914 \pm 0.20	4.89
2^{13}	0.614 \pm 0.06	2.18	0.711 \pm 0.08	2.52	0.810 \pm 0.10	2.76	0.910 \pm 0.18	4.42
2^{14}	0.611 \pm 0.05	1.83	0.710 \pm 0.10	3.15	0.790 \pm 0.07	1.98	0.910 \pm 0.09	2.21
2^{15}	0.606 \pm 0.02	0.74	0.707 \pm 0.02	0.63	0.808 \pm 0.03	0.83	0.906 \pm 0.04	0.99
2^{16}	0.605 \pm 0.02	0.74	0.707 \pm 0.03	0.95	0.803 \pm 0.03	0.84	0.904 \pm 0.03	0.74
2^{17}	0.602 \pm 0.01	0.37	0.707 \pm 0.02	0.63	0.801 \pm 0.02	0.56	0.898 \pm 0.02	0.50
Multifractal Detrended Fluctuation Analysis method								
2^{12}	0.628 \pm 0.19	6.77	0.744 \pm 0.17	5.11	0.825 \pm 0.15	3.12	0.850 \pm 0.18	4.74
2^{13}	0.627 \pm 0.19	6.78	0.726 \pm 0.11	3.39	0.822 \pm 0.10	2.79	0.876 \pm 0.06	1.53
2^{14}	0.594 \pm 0.09	3.39	0.714 \pm 0.08	2.50	0.812 \pm 0.09	1.51	0.889 \pm 0.06	1.51
2^{15}	0.599 \pm 0.02	0.75	0.708 \pm 0.03	0.95	0.792 \pm 0.03	0.85	0.897 \pm 0.03	0.75
2^{16}	0.601 \pm 0.01	0.37	0.704 \pm 0.02	0.64	0.807 \pm 0.02	0.55	0.908 \pm 0.03	0.74
2^{17}	0.600 \pm 0.01	0.37	0.703 \pm 0.01	0.32	0.805 \pm 0.02	0.56	0.905 \pm 0.01	0.25

3.1.2. Evaluation of the Wavelet-Based Methods

In order to determine the value of the Hurst exponent with this method, it is necessary to perform a discrete wavelet transformation to the investigated process, applying a wavelet algorithm and assigning scale values (i,j).

Due to the fact that the wavelet-based method does not offer a methodology for determining the size of the scale and the choice of the wavelet algorithm, in this paper two wavelet algorithms are investigated and compared in terms of the exact determination of the Hurst exponent: Haar and Daubechies at the following scale values (i,j): $1 \leq i \leq 6$, and

$j = 10$. The Daubechies algorithm was tested with the following wavelet coefficients: 4, 8, 10 and 12.

Table 2 shows the determined values and relative errors of the Hurst exponent of a simulated fractal process of length 2^{15} points using the two algorithms with different values of the wavelet scale.

Table 2. Determining the value and relative error of the Hurst exponent using a wavelet-based method.

Scale (i,j)	H = 0.6		H = 0.7		H = 0.8		H = 0.9	
	\hat{H} Mean \pm sd	RSE (%)	\hat{H} Mean \pm sd	RSE (%)	\hat{H} Mean \pm sd	RSE (%)	\hat{H} Mean \pm sd	RSE (%)
Haar algorithm								
(1,10)	0.596 \pm 0.06	2.25	0.698 \pm 0.06	1.92	0.801 \pm 0.07	1.95	0.904 \pm 0.08	1.98
(2,10)	0.596 \pm 0.04	1.50	0.699 \pm 0.04	1.27	0.803 \pm 0.04	1.11	0.906 \pm 0.06	1.48
(3,10)	0.598 \pm 0.05	1.87	0.702 \pm 0.05	1.59	0.806 \pm 0.05	1.39	0.911 \pm 0.05	1.23
(4,10)	0.599 \pm 0.06	2.24	0.705 \pm 0.07	2.22	0.811 \pm 0.06	1.65	0.917 \pm 0.07	1.71
(5,10)	0.607 \pm 0.07	2.57	0.714 \pm 0.06	1.88	0.821 \pm 0.07	1.91	0.927 \pm 0.09	2.17
(6,10)	0.597 \pm 0.06	2.25	0.711 \pm 0.06	1.89	0.824 \pm 0.08	2.17	0.936 \pm 0.10	2.39
Daubechies algorithm with 4 coefficients								
(1,10)	0.599 \pm 0.06	2.24	0.702 \pm 0.07	2.23	0.804 \pm 0.08	2.22	0.906 \pm 0.09	2.22
(2,10)	0.599 \pm 0.03	1.12	0.702 \pm 0.04	1.27	0.804 \pm 0.06	1.67	0.905 \pm 0.06	1.48
(3,10)	0.600 \pm 0.05	1.86	0.702 \pm 0.03	0.96	0.804 \pm 0.07	1.95	0.905 \pm 0.08	1.98
(4,10)	0.603 \pm 0.06	2.22	0.704 \pm 0.05	1.59	0.806 \pm 0.08	2.22	0.908 \pm 0.10	2.46
(5,10)	0.611 \pm 0.07	2.56	0.713 \pm 0.07	2.20	0.816 \pm 0.09	2.47	0.917 \pm 0.11	2.68
(6,10)	0.601 \pm 0.06	2.23	0.703 \pm 0.08	2.54	0.805 \pm 0.10	2.78	0.909 \pm 0.09	2.21
Daubechies algorithm with 8 coefficients								
(1,10)	0.610 \pm 0.05	1.83	0.713 \pm 0.07	2.20	0.815 \pm 0.09	2.47	0.916 \pm 0.10	2.44
(2,10)	0.612 \pm 0.04	1.46	0.714 \pm 0.06	1.87	0.815 \pm 0.07	1.92	0.915 \pm 0.08	1.96
(3,10)	0.615 \pm 0.06	2.18	0.717 \pm 0.07	2.18	0.817 \pm 0.8	2.19	0.916 \pm 0.09	2.20
(4,10)	0.625 \pm 0.12	4.29	0.727 \pm 0.10	3.08	0.827 \pm 0.12	3.24	0.926 \pm 0.14	3.38
(5,10)	0.638 \pm 0.19	6.66	0.739 \pm 0.18	5.45	0.839 \pm 0.17	4.53	0.936 \pm 0.19	4.54
(6,10)	0.661 \pm 0.25	8.46	0.763 \pm 0.26	7.62	0.862 \pm 0.27	7.00	0.957 \pm 0.23	5.37
Daubechies algorithm with 10 coefficients								
(1,10)	0.600 \pm 0.03	1.12	0.704 \pm 0.03	0.95	0.804 \pm 0.04	1.11	0.908 \pm 0.04	0.98
(2,10)	0.600 \pm 0.01	0.37	0.701 \pm 0.01	0.32	0.804 \pm 0.01	0.28	0.904 \pm 0.01	0.25
(3,10)	0.601 \pm 0.02	0.74	0.702 \pm 0.02	0.64	0.803 \pm 0.02	0.56	0.904 \pm 0.02	0.49
(4,10)	0.605 \pm 0.04	1.48	0.705 \pm 0.04	1.27	0.806 \pm 0.04	1.11	0.907 \pm 0.05	1.23
(5,10)	0.614 \pm 0.06	2.19	0.715 \pm 0.07	2.19	0.816 \pm 0.08	2.19	0.917 \pm 0.07	1.22
(6,10)	0.612 \pm 0.05	1.83	0.711 \pm 0.05	1.57	0.813 \pm 0.07	1.92	0.916 \pm 0.06	1.46
Daubechies algorithm with 12 coefficients								
(1,10)	0.601 \pm 0.02	0.74	0.705 \pm 0.03	0.95	0.808 \pm 0.04	1.11	0.911 \pm 0.05	1.23
(2,10)	0.600 \pm -0.01	0.37	0.704 \pm 0.01	0.32	0.807 \pm 0.03	0.83	0.908 \pm 0.04	0.98
(3,10)	0.601 \pm 0.01	0.37	0.704 \pm 0.01	0.32	0.807 \pm 0.03	0.83	0.908 \pm 0.04	0.98
(4,10)	0.696 \pm 0.03	0.96	0.710 \pm 0.05	1.57	0.813 \pm 0.06	1.65	0.916 \pm 0.07	1.71
(5,10)	0.618 \pm 0.07	2.53	0.722 \pm 0.09	2.79	0.826 \pm 0.12	3.25	0.928 \pm 0.14	3.37
(6,10)	0.626 \pm 0.09	3.21	0.734 \pm 0.13	3.96	0.842 \pm 0.18	4.78	0.948 \pm 0.23	5.42

Figure 2 shows the graph of the wavelet-based method using the Daubechies algorithm with 10 coefficients to determine the Hurst exponent of a generated fractal process with a length of 2^{15} (32,768) points and an input value of $H = 0.8$. The obtained value of the Hurst exponent is $\hat{H} = 0.8004$, and the relative error is $RSE(\%) = 0.05$.

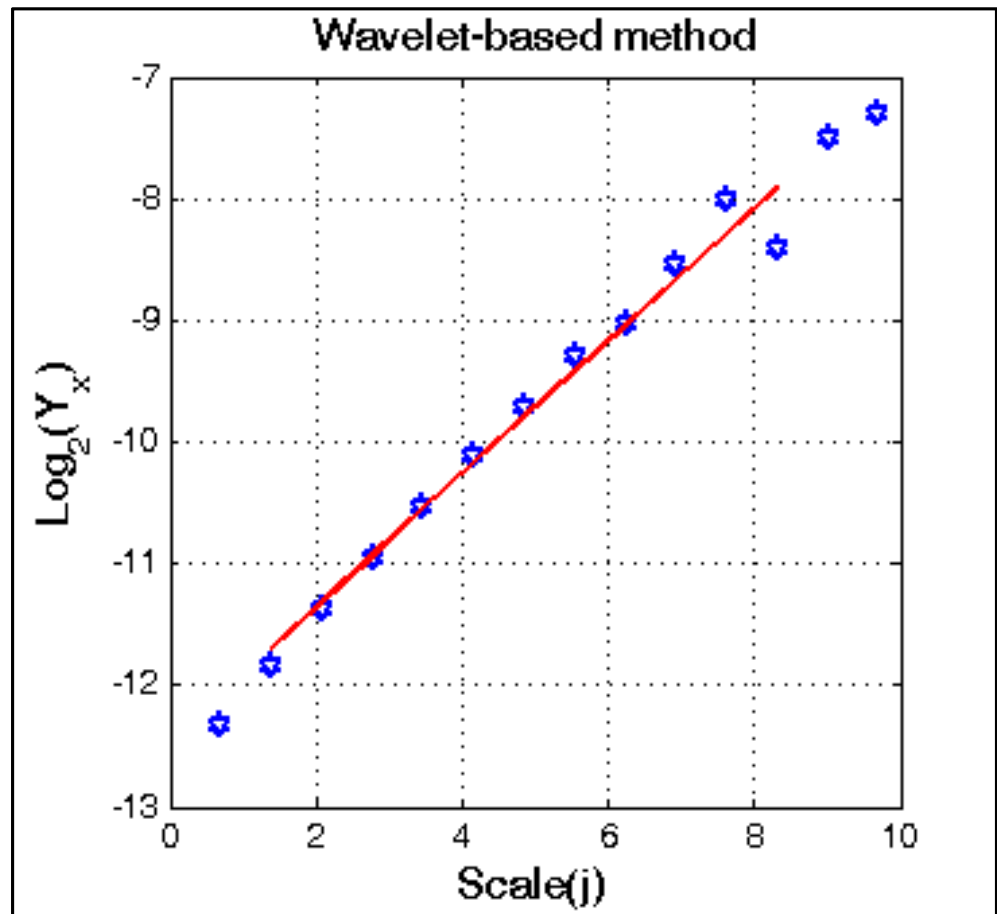


Figure 2. Wavelet-based method for determining the Hurst exponent.

Based on the obtained results, the following conclusions can be drawn about the wavelet-based method:

1. The RSE in determining the Hurst exponent using the Haar and Daubechies algorithms is the smallest when the scale is $(i,j) = (2,10)$ and $(i,j) = (3,10)$. In the article, when applying this method, the scale $(i,j) = (2,10)$ is used;
2. The RSE in determining the Hurst exponent is smaller when using the Daubechies algorithm compared to the Haar algorithm;
3. The RSE of the Hurst exponent is the smallest when using the Daubechies algorithm with 10 coefficients and it is less than 0.5%.

3.1.3. Evaluation of the DFA Method

Figure 3 shows how the fluctuations of a simulated fractal process ($H = 0.8$) are changed through the parameters α_1 , α_2 and α_{all} . The fluctuation function F_s at large values of the scale s increases according to the power law:

$$F_s \sim s^{H(q)} \tag{21}$$

where $H(q)$ is a scaling exponent.

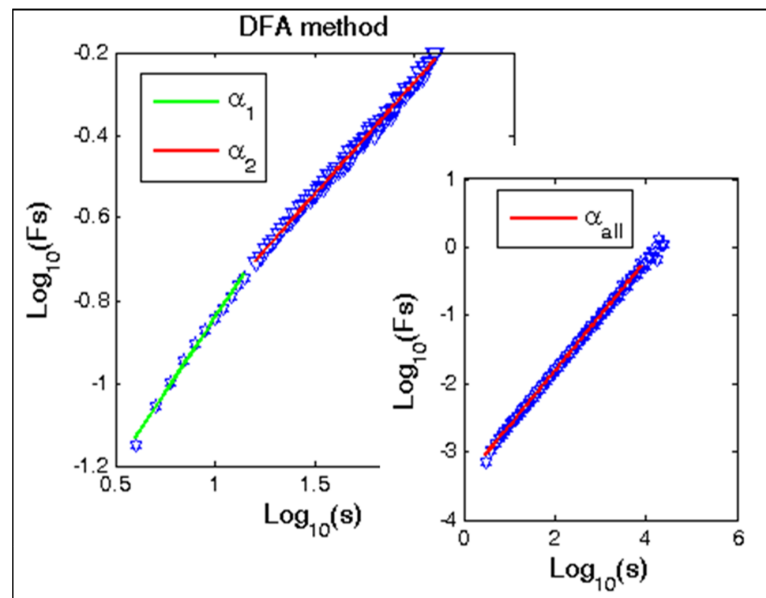


Figure 3. DFA method for determining the Hurst exponent.

The first part of the slope of the graph (colored in green) corresponds to the short-term fractal exponent $\alpha_1 = 0.8750$ for segments of size $4 < s < 16$, and the second part (colored in red) corresponds to the long-term fractal exponents $\alpha_2 = 0.8010$ for segment size $16 < s < 64$, and the parameter $\alpha_{all} = 0.8022$ corresponds to the Hurst exponent as the $RSE(\%) = 0.22$. The values of these parameters are evidence that the simulated process is fractal.

3.1.4. Evaluation of the MFDFA Method

To study the fractal behaviour of the simulated processes in relation to the Hurst exponent with the MFDFA method, the relationship between the generalized Hurst exponent H and the parameter q was determined. This connection is shown in Figure 4, from which it follows that the determined value of the generalized Hurst exponent is almost a constant quantity depending on q and this is a confirmation that the generated process is monofractal.

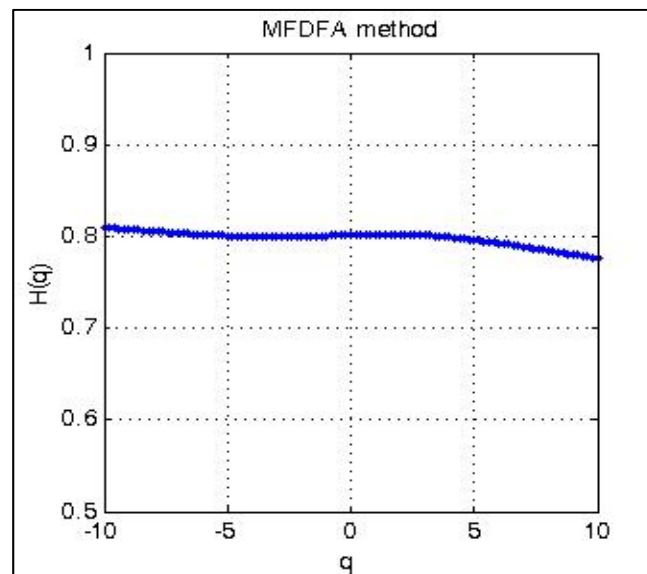


Figure 4. MFDFA method for determining the generalized Hurst exponent.

3.2. Analysis of Real Cardiological Data

In this paper, the following three methods were used to study the fractality of real cardiac data: wavelet-based, DFA and MFDFA, which were determined to have a high degree of accuracy in determining the Hurst exponent. The studied cardiological data refer to the intervals between heartbeats (RR interval series), with the help of which information related to the health status of the patients is obtained. For diagnostic purposes, these methods can be used both autonomously and in combination with other methods for monitoring the cardiovascular condition of patients.

The use of nonlinear statistical methods in cardiology, to which the proposed three methods also apply, is a relatively new trend. One of the advantages of these methods is that they can detect subtle changes in the dynamics of the RR interval series and with their help solve many prognostic and diagnostic tasks.

In Figure 5 shows the graphs of the dependence between the generalized Hurst exponent H and the parameter q for a healthy subject and for a patient with arrhythmia. In a healthy subject, the Hurst exponent changes for the different values of the parameter q , from which it follows that the process is multifractal, while in a sick patient, the Hurst exponent is almost a constant value, therefore the process is monofractal.

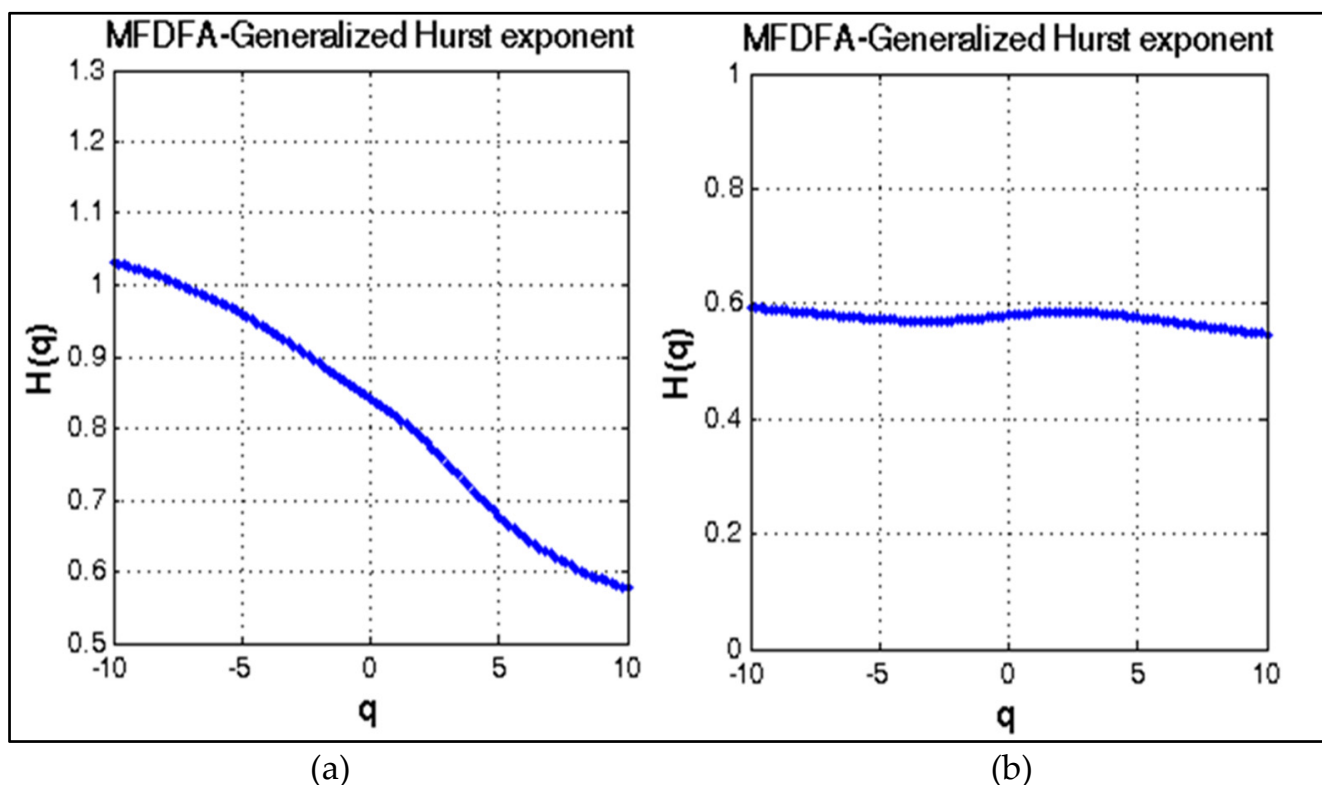


Figure 5. MFDFA method for determining the Hurst exponent (a) healthy subject with $H(q = 2) = 0.8192$ (b) sick patient (arrhythmia) with $H(q = 2) = 0.5892$.

Table 3 shows the results obtained through the methods used in the analysis of two groups of patients: healthy subjects and patients with arrhythmia. Results are shown as: mean \pm sd. The results show that the values of the studied parameters are lower in the patients with arrhythmia, and the p -values determined by t-test are less than 0.05. Therefore, the studied parameters of the three methods have statistical significance, which makes it possible to distinguish the two studied groups.

Table 3. Comparison between healthy and unhealthy subjects.

Parameter	Healthy Subject (Mean \pm sd) N = 48	Unhealthy Subject (Mean \pm sd) N = 48	p-Value
Hurst exponent	Wavelet-based method		0.0001
	0.8402 \pm 0.012	0.6019 \pm 0.010	
α_1 α_2 α_{all}	DFA method		0.0001
	1.0106 \pm 0.091	0.6079 \pm 0.046	
	0.7913 \pm 0.058	0.6923 \pm 0.082	
	0.8530 \pm 0.072	0.6150 \pm 0.071	0.0001
Generalized Hurst exponent at q = 2	MFDFA method		0.0001
	0.8201 \pm 0.031	0.5932 \pm 0.024	

4. Conclusions

In the present paper, the self-similarity property of fractal processes is determined by calculating the Hurst exponent of process fluctuations in order to obtain information on long-term correlations and to predict the behaviour of the studied processes. The theoretical and practical significance of the obtained results, which are part of the project “Investigation of the application of new mathematical methods for the analysis of cardiac data”, are concluded in studying the possibilities of using nonlinear statistical methods, such as: wavelet-based, DFA and MFDFA for the diagnosis of the cardiovascular condition of the human body. Changes in the body related to disease or under the influence of external factors lead to changes in heart rate variability, which as a rule have fractal behaviour. In this regard, the knowledge related to the fractal and multi-fractal features of cardiac signals can help doctors to correctly diagnose patients.

Interest in the use of electrocardiographic signals recorded by a Holter device for continuous 24-h monitoring of the cardiovascular state of the human organism has been continuously growing in recent years. This opportunity offers a range of science, technology, engineering and mathematics (STEM) skills and information designed not only for doctors but also for a wide range of people. Based on the information obtained related to cardiac health allows patients to learn to use and understand the electrical rhythms of the human body.

Future work related to the topic of the present paper is the analysis of the stress on heart rate variability. Two types of stressful situations will be explored. The first type of stress states will be simulated by playing 3D extreme games, and the second type will be real stress states that will be generated during sports training and fitness.

Author Contributions: Conceptualization, investigation and methodology, E.G. and P.L.; Create software for mathematical analysis of the fractal processes, G.G.-T. and E.G.; Validation, G.B.; Manuscript review and contribution to final version, G.B. and D.D. All authors have read and agreed to the published version of the manuscript.

Funding: This research was funded by NATIONAL SCIENCE FUND OF BULGARIA (scientific project “Investigation of the application of new mathematical methods for the analysis of cardiac data”), Grant Number KP-06-N22/5, 7 December 2018.

Institutional Review Board Statement: This study was approved by the Research Ethics Committee at Medical University—Varna, Bulgaria, Protocol/Decision No. 82, 28 March 2019.

Informed Consent Statement: All participants were informed in advance of the research that would be performed on them. Informed consent was obtained from all subjects involved in the study.

Data Availability Statement: A database of cardiac information (intervals between heartbeats-RR) was created for patients with various cardiovascular diseases: arrhythmia, heart failure, ischemia, syncope, and healthy controls. The database is located at: <http://hrvdata.vtlab.eu>. These data were taken at Medical University-Varna.

Acknowledgments: This research work was carried out as part of the scientific project “Investigation of the application of new mathematical methods for the analysis of cardiac data” No KP-06-N22/5, date 7 December 2018, funded by the National Science Fund of Bulgaria (BNSF).

Conflicts of Interest: The authors declare no conflict of interest.

References

1. Falconer, K.J. *Fractal Geometry: Mathematical Foundations and Applications*; John Wiley & Sons: Hoboken, NJ, USA, 2014.
2. Captur, G.; Karperien, A.L.; Hughes, A.D.; Francis, D.P.; Moon, J.C. The fractal heart—Embracing mathematics in the cardiology clinic. *Nat. Rev. Cardiol.* **2017**, *14*, 56–64. [[CrossRef](#)]
3. Kunz, V.C.; Borges, E.N.; Coelho, R.C.; Gubolino, L.A.; Martins, L.E.B.; Silva, E. Linear and nonlinear analysis of heart rate variability in healthy subjects and after acute myocardial infarction in patients. *Braz. J. Med. Biol. Res.* **2012**, *45*, 450–458. [[CrossRef](#)] [[PubMed](#)]
4. Andronache, I.C.; Peptenatu, D.; Ciobotaru, A.-M.; Gruia, A.K.; Nina Margareta Gropoșilă, N.M. Using Fractal Analysis in Modeling Trends in the National Economy. *Procedia Environ. Sci.* **2016**, *32*, 344–351. [[CrossRef](#)]
5. Wang, L.; He, K.; Zou, Y.; Feng, Z. Multiscale Fractal Analysis of Electricity Markets. In Proceedings of the Seventh International Joint Conference on Computational Sciences and Optimization, Beijing, China, 4–6 July 2014; pp. 378–382. [[CrossRef](#)]
6. Ouadfeul, S.; Aliouane, L.; Boudella, A. Fractal and Chaos in Exploration Geophysics. In *Fractal Analysis and Chaos in Geosciences*; IntechOpen: London, UK, 2012. [[CrossRef](#)]
7. Peng, C.K.; Havlin, S.; Stanley, H.E.; Goldberger, A.L. Quantification of scaling exponents and crossover phenomena in nonstationary heartbeat time series. *Chaos* **1995**, *5*, 82–87. [[CrossRef](#)]
8. Mariani, M.C.; Kubin, W.; Asante, P.K.; Tweneboah, O.K.; Beccar-Varela, M.P.; Jaroszewicz, S.; Gonzalez-Huizar, H. Self-Similar Models: Relationship between the Diffusion Entropy Analysis, Detrended Fluctuation Analysis and Lévy Models. *Mathematics* **2020**, *8*, 1046. [[CrossRef](#)]
9. Mariani, M.C.; Asante, P.K.; Bhuiyan, M.A.M.; Beccar-Varela, M.P.; Jaroszewicz, S.; Tweneboah, O.K. Long-Range Correlations and Characterization of Financial and Volcanic Time Series. *Mathematics* **2020**, *8*, 441. [[CrossRef](#)]
10. Suszyński, M.; Peta, K.; Černošák, V.; Svoboda, M. Mechanical Assembly Sequence Determination Using Artificial Neural Networks Based on Selected DFA Rating Factors. *Symmetry* **2022**, *14*, 1013. [[CrossRef](#)]
11. Mandelbrot, B. *The Fractal Geometry of Nature*; W H Freeman & Co.: New York, NY, USA, 1982.
12. Mandelbrot, B. *Fractals and Scaling in Finance*; Springer: New York, NY, USA, 1997.
13. Kale, M.; Butar, F.B. Fractal Analysis of Time Series and Distribution Properties of Hurst Exponent. *J. Math. Sci. Math. Educ.* **2007**, *5*, 8–19.
14. Sheluhin, O.I.; Smolskiy, S.M.; Osin, A.V. *Self-Similar Processes in Telecommunications*; John Wiley & Sons, Ltd.: Hoboken, NJ, USA, 2007.
15. Kantelhardt, J.W. Fractal and Multifractal Time Series. In *Mathematics of Complexity and Dynamical Systems*; Meyers, R., Ed.; Springer: New York, NY, USA, 2012. [[CrossRef](#)]
16. Nigmatullin, R.; Dorokhin, S.; Ivchenko, A. Generalized Hurst Hypothesis: Description of Time-Series in Communication Systems. *Mathematics* **2021**, *9*, 381. [[CrossRef](#)]
17. Raimundo, M.S.; Okamoto, J. Application of Hurst Exponent (H) and the R/S Analysis in the Classification of FOREX Securities. *Int. J. Modeling Optim.* **2018**, *8*, 116–124. [[CrossRef](#)]
18. Li, J.; Chen, Y. Rescaled range (R/S) analysis on seismic activity parameters. *Acta Seimol. Sin.* **2008**, *14*, 148–155. [[CrossRef](#)]
19. Schandrasekaran, S.; Poomalai, S.; Saminathan, B.; Suthanthiravel, S.; Sundaram, K.; Hakkim, F.F.A. An investigation on the relationship between the Hurst exponent and the predictability of a rainfall time series. *Meteorol. Appl.* **2019**, *26*, 511–519. [[CrossRef](#)]
20. Quanmin, B.; Jun, B.; Zengwei, Y.; Lei, H. R/S method for evaluation of pollutant time series in environmental quality assessment. *Water Sci. Eng.* **2008**, *1*, 82–88. [[CrossRef](#)]
21. Li, Y.; Teng, Y. Estimation of the Hurst Parameter in Spot Volatility. *Mathematics* **2022**, *10*, 1619. [[CrossRef](#)]
22. Kaminskiy, R.; Shakhovska, N.; Kajanová, J.; Kryvenchuk, Y. Method of Distinguishing Styles by Fractal and Statistical Indicators of the Text as a Sequence of the Number of Letters in Its Words. *Mathematics* **2021**, *9*, 2410. [[CrossRef](#)]
23. Ghosh, B.; Bouri, E. Is Bitcoin’s Carbon Footprint Persistent? Multifractal Evidence and Policy Implications. *Entropy* **2022**, *4*, 647. [[CrossRef](#)]
24. Cornforth, D.; Jelinek, H.F.; Tarvainen, M. A Comparison of Nonlinear Measures for the Detection of Cardiac Autonomic Neuropathy from Heart Rate Variability. *Entropy* **2015**, *17*, 1425–1440. [[CrossRef](#)]
25. Liu, K.; Zhang, X.; Chen, Y. Extraction of Coal and Gangue Geometric Features with Multifractal Detrending Fluctuation Analysis. *Appl. Sci.* **2018**, *8*, 463. [[CrossRef](#)]
26. Stosic, D.; Stosic, D.; Vodenska, I.; Stanley, H.E.; Stosic, T. A New Look at Calendar Anomalies: Multifractality and Day-of-the-Week Effect. *Entropy* **2022**, *24*, 562. [[CrossRef](#)]
27. Miloš, L.R.; Hačigan, C.; Miloš, M.C.; Barna, F.M.; Boțoc, C. Multifractal Detrended Fluctuation Analysis (MF-DFA) of Stock Market Indexes. Empirical Evidence from Seven Central and Eastern European Markets. *Sustainability* **2020**, *12*, 535. [[CrossRef](#)]

28. Abundo, M.; Pirozzi, E. On the Integral of the Fractional Brownian Motion and Some Pseudo-Fractional Gaussian Processes. *Mathematics* **2019**, *7*, 991. [[CrossRef](#)]
29. Yan, Z.; Guirao, J.L.G.; Saeed, T.; Chen, H.; Liu, X. Different Stochastic Resonances Induced by Multiplicative Polynomial Trichotomous Noise in a Fractional Order Oscillator with Time Delay and Fractional Gaussian Noise. *Fractal Fract.* **2022**, *6*, 191. [[CrossRef](#)]
30. Kermarrec, G. On Estimating the Hurst Parameter from Least-Squares Residuals. Case Study: Correlated Terrestrial Laser Scanner Range Noise. *Mathematics* **2020**, *8*, 674. [[CrossRef](#)]
31. Golmankhaneh, A.K.; Sibatov, R.T. Fractal Stochastic Processes on Thin Cantor-Like Sets. *Mathematics* **2021**, *9*, 613. [[CrossRef](#)]
32. Acharya, U.R.; Suri, J.S.; Spaan, J.A.E.; Krishnan, S.M. *Advances in Cardiac Signal Processing*; Springer: Berlin/Heidelberg, Germany, 2007.
33. Ernst, G. *Heart Rate Variability*; Springer: London, UK, 2014.
34. Malik, M. Task Force of the European Society of Cardiology and the North American Society of Pacing and Electrophysiology, Heart rate variability—Standards of measurement, physiological interpretation, and clinical use. *Circulation* **1996**, *93*, 1043–1065. [[CrossRef](#)]
35. Sen, J.; McGill, D. Fractal analysis of heart rate variability as a predictor of mortality: A systematic review and meta-analysis. *Interdiscip. J. Nonlinear Sci.* **2018**, *28*, 072101. [[CrossRef](#)]
36. Brockwell, P.; Davis, R. *Time Series: Theory and Methods*, 2nd ed.; Springer: New York, NY, USA, 1991.
37. Taqqu, M.; Willinger, W.; Sherman, R. Proof of a Fundamental Result in Self-Similar Traffic Modeling. *Comput. Commun. Rev.* **1997**, *27*, 5–23. [[CrossRef](#)]
38. Hosking, J.R. Modeling persistence in hydrological time series using fractional differencing. *Water Resour. Res.* **1984**, *20*, 1898–1908. [[CrossRef](#)]
39. Fei, Y.; Shao, X.; Wang, G.; Zhou, L.; Xia, X.; He, Y. Effectiveness of Electricity Derivatives Market Based on Hurst Exponent. In Proceedings of the 4th International Conference on Advances in Energy and Environment Research (ICAER 2019), Shanghai, China, 16–18 August 2019. 4p. [[CrossRef](#)]
40. Hurst, H.E. Long-Term Storage Capacity of Reservoirs. *Trans. Am. Soc. Civil Eng.* **1951**, *116*, 770–799. [[CrossRef](#)]
41. Hurst, H.E.; Black, R.P.; Simaika, Y.M. *Long-Term Storage: An Experimental Study*; Constable: London, UK, 1965.
42. Cohen, A.; Atoui, M.A.A. On Wavelet-based Statistical Process Monitoring. *Trans. Inst. Meas. Control* **2022**, *44*, 525–538. [[CrossRef](#)]
43. Muzy, J.F.; Bacry, E.; Arneodo, A. The Multifractal Formalism Revisited with Wavelets. *Int. J. Bifurc. Chaos* **1994**, *4*, 245–302. [[CrossRef](#)]
44. Mahmoud, M.; Dessouky, M.; Deyab, S.; Elfouly, F. Comparison between Haar and Daubechies Wavelet Transformations on FPGA Technology. World Academy of Science, Engineering and Technology, Open Science Index 2. *Int. J. Aerosp. Mech. Eng.* **2007**, *1*, 141–145.
45. Sharif, I.; Khare, S. Comparative Analysis of Haar and Daubechies Wavelet for Hyper Spectral Image Classification. *ISPRS Int. Arch. Photogramm. Remote Sens. Spat. Inf. Sci.* **2014**, *8*, 937–941.
46. Kusi, B. Performance Analysis between Haar and Daubechies Discrete Wavelet Transform in Digital Watermarking. *Int. J. Adv. Eng.* **2019**, *2*, 17–26.
47. Mahmoud, W.A.; Hadi, A.S.; Jawad, T.M. Development of a 2-D Wavelet Transform based on Kronecker Product. *J. Al-Nahrain Univ.* **2012**, *15*, 208–213. [[CrossRef](#)]
48. Maraun, D.; Rust, H.W.; Timmer, J. Tempting long-memory—On the interpretation of DFA results. *Nonlinear Processes Geophys.* **2004**, *11*, 495–503. [[CrossRef](#)]
49. Golińska, A.K. Detrended Fluctuation Analysis (DFA) in Biomedical Signal Processing: Selected Examples. *Stud. Logic Gramm. Rhetor.* **2012**, *29*, 107–115.
50. Kantelhardt, J.W.; Zschiegner, S.A.; Koscielny-Bunde, E.; Havlin, S.; Bunde, A.; Stanley, H.E. Multifractal detrended fluctuation analysis of nonstationary time series. *Phys. A Stat. Mech. Appl.* **2002**, *316*, 87–114. [[CrossRef](#)]
51. Kamath, M.V.; Watanabe, M.A.; Upton, A.R.M. (Eds.) *Heart Rate Variability (HRV) Signal Analysis: Clinical Applications*; CRC Press: Boca Raton, FL, USA; Taylor & Francis Group: Abingdon, UK, 2016.
52. Kalisky, T.; Ashkenazy, Y.; Havlin, S. Volatility of fractal and multifractal time series. *Israel J. Earth Sci.* **2007**, *65*, 47–56. [[CrossRef](#)]